

Human Pose Transfer with Augmented Disentangled Feature Consistency

Kun Wu, Chengxiang Yin, *Student Member, IEEE*, Zhengping Che, *Member, IEEE*, Bo Jiang, Jian Tang, *Fellow, IEEE*, Zheng Guan, *Member, IEEE*, and Gangyi Ding, *Senior Member, IEEE*

Abstract—Deep generative models have made great progress in synthesizing images with arbitrary human poses and transferring poses of one person to others. Though many different methods have been proposed to generate images with high visual fidelity, the main challenge remains and comes from two fundamental issues: pose ambiguity and appearance inconsistency. To alleviate the current limitations and improve the quality of the synthesized images, we propose a pose transfer network with augmented Disentangled Feature Consistency (DFC-Net) to facilitate human pose transfer. Given a pair of images containing the source and target person, DFC-Net extracts pose and static information from the source and target respectively, then synthesizes an image of the target person with the desired pose from the source. Moreover, DFC-Net leverages disentangled feature consistency losses in the adversarial training to strengthen the transfer coherence and integrates a keypoint amplifier to enhance the pose feature extraction. With the help of the disentangled feature consistency losses, we further propose a novel data augmentation scheme that introduces unpaired support data with the augmented consistency constraints to improve the generality and robustness of DFC-Net. Extensive experimental results on MIXAMO-POSE and EDN-10K have demonstrated DFC-Net achieves state-of-the-art performance on pose transfer.

Index Terms—Human pose transfer, Generative adversarial network, Image generation, Computer vision

I. INTRODUCTION

HUMAN pose transfer has become increasingly compelling recently since it is closely related to movies' special effects [1], reenactment [2], person re-identification [3], entertainment systems [4] and so forth [5], [6]. Given some images of a target person and a source person image with the desired pose (e.g., judo, dance), the goal of the human pose transfer task is to synthesize a realistic image of the target person with the desired pose of the source person.

With the power of deep learning, especially the generative adversarial networks (GANs) [7], pioneering works have raised impressive solutions to address the human image generation [8], [9], [10], [6] by efficiently leveraging the image-to-image translation schemes and have achieved significant progress. Intuitively, early routine coarsely conducts

human pose transfer through general image-to-image translation methods such as Pix2Pix [11] and CycleGAN [12], which attempt to translate the extracted skeleton image of source person to the image of target person with the desired poses.

Subsequent approaches [13], [14], [15] adopt specifically designed modules for human pose transfer. Specifically, the U-net architecture with skip connections in [16] is employed to keep the low-level features. To mitigate the pose misalignment between the source and target persons, [17] uses part-wise affine transformation with a modified feature fusion mechanism to warp the appearance features onto the target pose. Later, extensive works have been presented to strengthen the modeling ability of body deformation and feature transfer with different methods, including 3D surface models [18], [15], [19], local attention [20], [21] and optical flow [22]. However, the warping methods commonly struggle with *pose ambiguity* when viewpoint changes, occlusions occur, or even transferring a complicated pose in many situations. To address the pose ambiguity, a series of works [22], [23] use predictive branch to illuminate and replenish new contents for invisible regions. When the hallucinated contents have a different context style than the local-warped ones, generated images will have a low visual fidelity due to *appearance inconsistency*. One of the main reasons for pose ambiguity and appearance inconsistency is that the commonly used reconstruction loss and the adversarial generative loss only constrain the synthesized image generation in image-level.

Towards alleviating the mentioned limitations, it is important to disentangle the pose and appearance information, and exploit the disentangled pose and appearance feature consistencies between the synthesized and real images, i.e., the synthesized target image should have a similar high-level appearance feature to the real target person as well as a similar high-level pose feature to the real source person. The disentangled pose and appearance feature consistencies can constrain the training in feature-level and lead to a more consistent and realistic synthesized result.

In this paper, we propose a pose transfer network with augmented Disentangled Feature Consistency (DFC-Net) to facilitate human pose transfer. DFC-Net contains a pose feature encoder and a static feature encoder to extract pose and appearance features from the source and target person, respectively. In pose feature encoder, we integrated a pre-trained pose estimator such as OpenPose [24] to extract the keypoint heatmaps. Notice that the pose estimator is pre-trained on COCO keypoint challenge dataset [25], which is not any dataset deployed in our experiments. Further, in order

Kun Wu and Chengxiang Yin are with Department of Electrical Engineering and Computer Science, Syracuse University, Syracuse, NY, 13244. E-mail: kwu102@syr.edu and cyin02@syr.edu

Zhengping Che and Jian Tang are with Midea Group, China. E-mail: chezp@midea.com and tangjian22@midea.com

Bo Jiang is with Didi Chuxing, China. E-mail: scottjiangbo@didiglobal.com

Zheng Guan and Gangyi Ding are with the Computer Science School, Beijing Institute of Technology, China. E-mail: guanzheng_bit@hotmail.com and dinggangyi_bit@hotmail.com

Corresponding author: Jian Tang

to remedy the distortion of the extracted keypoints caused by the distribution shift from pose estimator, we introduce a keypoint amplifier to eliminate the noise in keypoint heatmaps. An image generator synthesizes a realistic image of the target person conditioned on the disentangled pose and appearance features. The feature encoders and image generator empower DFC-Net to enable us to present novel feature-level pose and appearance consistency losses [12]. These losses reinforce the consistency of pose and appearance information in the feature space and simultaneously maintain visual fidelity. Additionally, to further improve the robustness and generality of DFC-Net, by disentangling the pose information from different source persons, we present a novel data augmentation scheme that builds an extra unpaired support dataset as the source images, which provides different persons with unseen poses in the training set and augmented consistency constraints.

We also notice that the commonly used datasets and benchmarks [26], [27] only focus on the persons in the real world with a low-resolution, which is not sufficient to verify the effectiveness of each algorithm on other domains, such as computer animation [28]. Inspired by [28], we collect an animation character image dataset named MIXAMO-POSE from Adobe Mixamo [29], a 3D animation library, to accurately generate different characters performing the identical poses as a benchmark to assess the human pose transfer between different people. MIXAMO-POSE contains four different animation characters performing 15 kinds of poses. To further evaluate the DFC-Net, we also modify a real person dataset called EDN-10K upon [30], which contains 10K high-resolution images for four real subjects performing different poses. The experimental results on these two datasets demonstrate that our model can effectively synthesize realistic images and conduct pose transfer for both the animation characters and real persons.

In summary, our contributions are as follows:

- We propose a novel method DFC-Net for human pose transfer with two disentangled feature consistency losses to make the information between the real images and synthesized images consistent.
- We propose a novel data augmentation scheme that enforces augmented consistency constraints with an unpaired support dataset to further improve the generality of our model.
- We collect an animation character dataset MIXAMO-POSE as a new benchmark to enable the accurate evaluation of pose transfer between different people on animation domain.
- We conduct extensive experiments on datasets MIXAMO-POSE and EDN-10K, on which the empirical results demonstrate the effectiveness of our method.

II. RELATED WORK

Generative adversarial networks (GANs) [7] have achieved tremendous success in image-to-image translation tasks, whose goal is to convert images from one domain to a different domain. Pix2Pix [11] proposes a framework based on cGANs [31] with an encoder-decoder architecture [32]; CycleGAN [12] addressed this problem by using a cycle-consistent

GANs; DualGAN [33] and [34] are also unsupervised image-to-image translation methods trained on unpaired dataset. Similarly, [35], [36], [37] are also image-to-image translation techniques, but they try to generate a dataset of the target domain with labels for domain adaptation tasks. The above works can be exploited as a general approach in the human pose transfer task, while the precondition is that they have a specific image domain which can be converted to the synthesized image domain, e.g., using a pose estimator [38] to generate a paired skeleton image dataset. Different from the image-to-image translation methods, DFC-Net improved the quality of the synthesized image by adding consistency constraints in the feature space.

Recently, there is a growing number of human pose transfer methods with specifically designed modules. One branch is the spatial transformation methods [17], [39], [15], aiming to build the deformation mapping of the keypoint correspondences in the human body. By leveraging the spatial transformation capability of CNN, [40] presented the spatial transformer networks (STN) that approximate the global affine transformation to warp the features. Following STN, several variant works [41], [42], [43] have been proposed to synthesize images with better performance. [44] used image segmentation to decompose the problem into modular subtasks for each body part and then integrated all parts into the final result. [17] built deformable skip connections to move information and transfer textures for pose transfer. Monkey-Net [45] encoded pose information via dense flow fields generated from keypoints learned in a self-supervised fashion. First-Order Motion Model [46] decoupled appearance and pose and proposes to use learned keypoints and local affine transformations to generate image animation. [23] integrated the human pose transfer, appearance transfer and novel view synthesis into one unified framework by using SMPL [47] to generate human body mesh. The spatial transformation methods usually implicitly assume that the warping operation can cover the whole body. However, when viewpoint changes and occlusions occur, the above assumption can not hold, leading to *pose ambiguity* and performance dropping.

Another branch methods are pose-guided and aim to predict new appearance contents in uncovered regions to handle the pose ambiguity problem. One of the earliest works, PG² [13], presented a two-stage method using U-Net to synthesize the target person with arbitrary poses. [14] further decomposed the image into the foreground, background and pose features to achieve more precise control of different information. [48] introduced a multi-stage GAN loss and synthesized each body part, respectively. [18] leveraged the DensePose [49] rather than the commonly used 2D key-points to perform accurate pose transfer. [30] learned a direct mapping from the skeleton images to synthesized images with corresponding pose based on the architecture of Pix2PixHD [50]. PATH [20] introduced cascaded attention transfer blocks (PATBs) to refine pose and appearance features simultaneously. Inspired by PATH, PMAN [51] proposed a progressive multi-attention framework with memory network to improve the image quality. However, some of these methods [18], [52], [22] focused on synthesizing results at the image level (i.e., adversarial and reconstruction

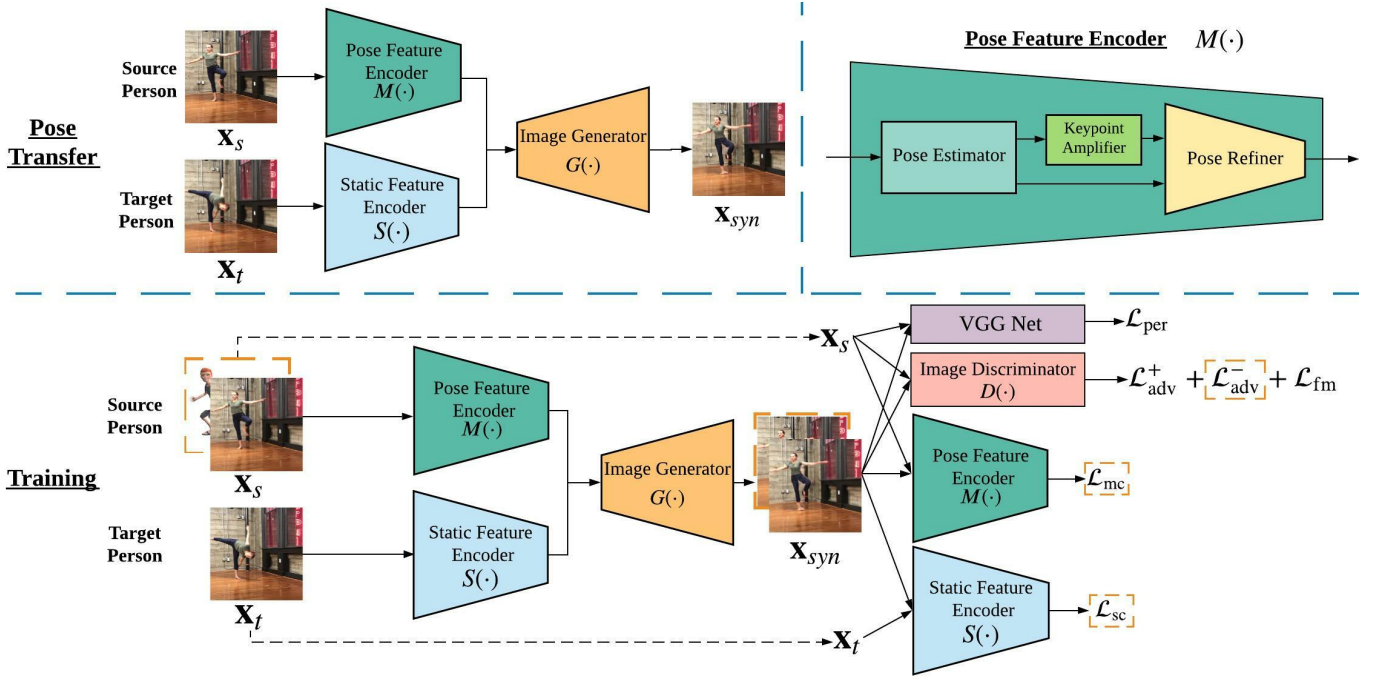


Fig. 1: **Upper left:** DFC-Net synthesizes an image of the target person performing the pose of the source person. **Upper right:** the Pose Feature Encoder $M(\cdot)$ includes three components: pre-trained Pose Estimator, Keypoint Amplifier and Pose Refiner. **Bottom:** the overview of training process of DFC-Net. Note that the images x_s surrounded by orange dotted boxes is from the support set, and the augmented consistency losses \mathcal{L}_{sup} are sum of $\mathcal{L}_{\text{adv}}^-$, \mathcal{L}_{mc} and \mathcal{L}_{sc} surrounded by orange dotted boxes.

losses), thus leading to appearance inconsistency when predicted local contents are not consistent with the surrounding contexts.

In contrast, our method learns to disentangle and reassemble the pose and appearance in the feature space. One similarly work close to ours is C²GAN [53] which consists of three generation cycles (i.e., one for image generation and two for keypoint generation). C²GAN explored the cross-modal information in the image-level at the cost of model complexity and training instability while DFC-Net only introduced two feature consistency losses into the full objective, which kept the model simple and effective. By disentangling the pose and appearance features, we can enforce the feature consistencies between the synthesized and real images, and leverage the pose features from an unpaired dataset to improve performance.

III. METHODOLOGY

A. Overview

Given one image x_s of a source person and another image x_t of a target person, DFC-Net synthesizes an image x_{syn} , which reserves a) the pose information, e.g., pose and location, of the source person in x_s , and b) the static information, e.g., person appearance and environment background, from the target image x_t . For each image, DFC-Net attempts to disentangle the pose and static information into orthogonal features. Specifically, DFC-Net consists of the following core components: 1) a *Pose Feature Encoder* $M(\cdot)$, which extracts pose features $M(x)$ from an image x ; 2) a *Static Feature Encoder* $S(\cdot)$, which extracts static features $S(x')$ from an

image x' ; and 3) an *Image Generator* $G(\cdot)$, which synthesizes an image $G(M(x), S(x'))$ based on the encoded pose and static features $M(x)$ and $S(x')$ separately.

In the remainder of this section, we describe the model architecture and introduce the training procedure, followed by the model instantiations.

B. Pose Transfer Network Architecture

The architecture of the proposed model is shown in Figure 1.

1) *Pose Feature Encoder*: Our designed Pose Feature Encoder consists of a Pose Estimator network, a Keypoint Amplifier block, and a Pose Refiner network. Given a RGB image $x \in \mathbb{R}^{3 \times H \times W}$ of height H and width W , the pre-trained *Pose Estimator* aims at extracting pose information $P(x)$ from the image x . Similar to [38], the extracted pose information contains the downsampled keypoint heatmaps $h \in \mathbb{R}^{18 \times \frac{H}{8} \times \frac{W}{8}}$ and the part affinity fields $p \in \mathbb{R}^{38 \times \frac{H}{8} \times \frac{W}{8}}$. The keypoint heatmaps h store the heatmaps of 18 body parts, and the part affinity fields p store the location and orientation for heatmaps of body parts and background, which has 38 ($= (18 + 1) \times 2$) channels.

As the pre-trained pose estimator (OpenPose [24] in our implementation) is pre-trained on COCO keypoint challenge dataset [25], when applied on MIXAMO-POSE and EDN-10K datasets with different distributions, more noise are made on keypoint heatmaps h . To reduce the interference of noise, we apply a softmax function with a relatively small temperature T (e.g., 0.01) as the *Keypoint Amplifier* to denoise the extracted keypoint heatmaps by increasing the gap between large

and small values in the heatmaps and obtain the amplified heatmaps \mathbf{h}' by

$$\mathbf{h}' = \text{softmax} \left(\frac{1}{T} \cdot \mathbf{h} \right). \quad (1)$$

By employing Keypoint Amplifier on the input heatmaps, the small probability, e.g., 0.2, will be squeezed to almost 0.0. On the contrary, the large probability, e.g., 0.8, will be squeezed to almost 1.0. Without the Keypoint Amplifier, the generator may still synthesize blurry limbs for the low probability areas and twist the generated person.

Finally, the *Pose Refiner* takes both the part affinity fields \mathbf{p} and the amplified keypoint heatmaps \mathbf{h}' and produces the encoded pose feature vector $M(\mathbf{x})$. In this way, the pose information extracted from the Pose Estimator can be refined, and the influence caused by different limb ratios and/or camera angles and distances can be reduced.

2) *Static Feature Encoder*: While the Pose Feature Encoder is not capable of extracting static information, the static information including background, personal appearance, etc., from another image \mathbf{x}' , are captured automatically by another module with the help of the full objective function. Named as Static Feature Encoder, this module extracts only static features $S(\mathbf{x}')$ from \mathbf{x}' .

3) *Image Generator*: Given pose features $M(\mathbf{x}_s)$ extracted from a source image \mathbf{x}_s and static features $S(\mathbf{x}_t)$ extracted from a target image \mathbf{x}_t , the Image Generator outputs the synthesized image \mathbf{x}_{syn} by

$$\mathbf{x}_{\text{syn}} = G(M(\mathbf{x}_s), S(\mathbf{x}_t)). \quad (2)$$

It is noting that many existing methods (e.g., [30]) attempt to learn pose-to-image or pose-to-appearance mapping solely via its generator, which is a difficult task on parameterizing the static information of the target in the generator. Meanwhile, with the same generator, the desired pose information of \mathbf{x}_s may fail to synthesize if the desired pose is very different from the training poses. DFC-Net, instead, extracts and utilizes decomposed static and pose features, which enables the reconstruction’s quality improvement.

C. Training DFC-Net

We train the pose transfer network in an adversarial learning way with disentangled feature consistency losses as well as other objectives. Basically, the model is trained with a set of images of the same person, possibly from one or several video clips. To further improve the generalization ability of DFC-Net, we propose to train DFC-Net with a support set and the augmented consistency losses. We show the ablation study results in Section IV-C.

1) *Adversarial Training*: We employ an *Image Discriminator* (D) in an adversarial learning way to ensure the synthesized image \mathbf{x}_{syn} borrows the pose and static information from the source and target images (\mathbf{x}_s and \mathbf{x}_t) separately. As both the source and target images during training contain the same person with the same appearance and background, they share almost the same static features, i.e., $S(\mathbf{x}_t) \simeq S(\mathbf{x}_s)$. Therefore, the output of the model \mathbf{x}_{syn} can also be treated

as a reconstruction of the source image \mathbf{x}_s , as the synthesized images contain the same pose features $M(\mathbf{x}_s)$ as the source image. This inspires us to resort to the conditional generative adversarial network (cGAN) [11], where the Image Discriminator attempts to discern between the real sample \mathbf{x}_s and the generated image \mathbf{x}_{syn} , conditioned on the pose features $M(\mathbf{x}_s)$ extracted from the source image. That is, the Image Discriminator attempts to fit $D(\mathbf{x}_s, M(\mathbf{x}_s)) = 1$ and $D(\mathbf{x}_{\text{syn}}, M(\mathbf{x}_s)) = 0$. The adversarial loss is described as follows:

$$\mathcal{L}_{\text{adv}} = -(\mathcal{L}_{\text{adv}}^+ + \mathcal{L}_{\text{adv}}^-), \quad (3)$$

where

$$\mathcal{L}_{\text{adv}}^+ = \log D(\mathbf{x}_s, M(\mathbf{x}_s)), \quad (4)$$

$$\mathcal{L}_{\text{adv}}^- = \log(1 - D(\mathbf{x}_{\text{syn}}, M(\mathbf{x}_s))). \quad (5)$$

We enhance the Image Discriminator with a multi-scale discriminator $D = (D_1, D_2)$ [50] and include the discriminator feature matching loss \mathcal{L}_{fm} in our objective. The feature matching loss is a weighted sum of feature losses from 5 different layers of the Image Discriminator, calculated by L_1 distance between the corresponding features of \mathbf{x}_s and \mathbf{x}_{syn} .

In order to increase the training stability and improve the synthesized image quality, we also add the perceptual loss \mathcal{L}_{per} [54] based on a pre-trained VGG network [55].

2) *Disentangled Feature Consistency Losses*: The above adversarial training losses aim at penalizing discrepancy between the synthesized and source images directly in the raw image space. To improve the accuracy and robustness of the pose transfer results, we also introduce two disentangled feature consistency losses in terms of *pose* and *static* features to assure the synthesized person looks like the target person and behaves as the source person separately. The pose consistency loss \mathcal{L}_{mc} measures the differences between the synthesized and source images in the pose feature space, and the static consistency loss \mathcal{L}_{sc} measures the differences between the synthesized and target images in the static feature space. They are both L_1 distances between the outputs from the corresponding encoders, formally defined as

$$\mathcal{L}_{\text{mc}} = \|M(\mathbf{x}_{\text{syn}}) - M(\mathbf{x}_s)\|_1, \quad (6)$$

$$\mathcal{L}_{\text{sc}} = \|S(\mathbf{x}_{\text{syn}}) - S(\mathbf{x}_t)\|_1. \quad (7)$$

3) *Augmented Consistency Loss*: Through disentangling the pose feature from the source images, we find that images with different persons can also be passed into the training process as the source images \mathbf{x}_s to improve the generalization ability of our model. Hence, we introduce a novel data augmentation method that extends the training dataset with the images of different persons, referred to as the *support set*, providing many kinds of unseen poses. Note that the subjects in *support set* can be arbitrary and are different from the primary training dataset, so the ground-truth images with the target person performing the pose of the source person are not available at all. As a result, the corresponding losses $\mathcal{L}_{\text{adv}}^+$, \mathcal{L}_{per} and \mathcal{L}_{fm} for the support set are not applicable, and we optimize relevant objective terms, which is defined by

$$\mathcal{L}_{\text{sup}} = \lambda_{\text{adv}} \mathcal{L}_{\text{adv}}^- + \lambda_{\text{mc}} \mathcal{L}_{\text{mc}} + \lambda_{\text{sc}} \mathcal{L}_{\text{sc}} \quad (8)$$

where the weights λ_{adv} , λ_{mc} , λ_{sc} are the weights for each loss.

4) *Full Objective*: By bringing all the objective terms together, we train all components jointly except for the Pose Estimator to minimize the full objective $\mathcal{L}_{\text{full}}$ below.

$$\begin{aligned} \mathcal{L}_{\text{full}} = & \lambda_{\text{adv}} \mathcal{L}_{\text{adv}} + \lambda_{\text{fm}} \mathcal{L}_{\text{fm}} + \lambda_{\text{per}} \mathcal{L}_{\text{per}} \\ & + \lambda_{\text{mc}} \mathcal{L}_{\text{mc}} + \lambda_{\text{sc}} \mathcal{L}_{\text{sc}} + \mathcal{L}_{\text{sup}} \end{aligned} \quad (9)$$

where λ_{adv} , λ_{fm} , λ_{per} are set to 1, 10, 10 following Pix2Pix [11] and Everybody Dance Now (EDN) [30], while λ_{mc} , λ_{sc} are set to 0.1, 0.01 by grid search. We set the λ_{sc} to 0.01 comparing to the λ_{mc} to balance the \mathcal{L}_{mc} and \mathcal{L}_{sc} .

D. Training and Inference Process

For each subject in the training dataset (i.e., MIXAMO-POSE and EDN-10K in our experiments), we train one separate model following the same scheme of [30] (e.g., we trained four models for four subjects in EDN-10k dataset.) For the sake of comparison fairness, we also train all the baseline methods following the same scheme.

During the training stage, given a training dataset consisting of N images of one subject and a support set, for each training iteration, we randomly choose a pair of images as x_s and x_t from the training dataset and an image as x_s from the support set respectively, pass them into the DFC-Net and train it using the full objective in Equation 9.

During the inference stage, given a desired pose image x_s , we randomly choose an image x_t from the training dataset and synthesize the result.

E. Implementation details

We employed the pre-trained VGG-19 [56] network part from [38] for the Pose Estimator, and adopted the similar approach in [22] to build our network, the detailed designs are as follows:

- **Pose Refiner**: It is composed of a convolutional block, a channel-wise upsampling module and five residual blocks [57]. Firstly, the convolutional block consists of a reflection padding layer, a 7×7 convolutional layer, a batch normalization layer and ReLU. The channel-wise upsampling module, which increases the number of the channel from 64 to 512, contains three convolutional blocks. Each block contains a 3×3 convolutional layer, a batch normalization layer and ReLU. Each of the five residual blocks consists of two small convolutional blocks and each block has a reflection padding layer, a 3×3 convolutional layer, a batch normalization layer. The first small convolutional block also has a ReLU at the end.
- **Static Feature Encoder**: It firstly has the same convolutional block as in the Pose Refiner. Then it contains three convolutional downsampling blocks and each block consists of a 3×3 convolutional layer, a batch normalization layer and ReLU. There are also five residual blocks

following the downsampling blocks as the same as in the Pose Refiner.

- **Image Generator**: It is composed of four residual blocks, an upsampling module and a convolutional block. Each of the residual blocks is the same as in the Pose Refiner and Static Feature Encoder. The upsampling module consists of three transposed convolutional blocks and each block is composed of a 3×3 transposed convolutional layer, a batch normalization layer and ReLU. The last convolutional block contains two reflection padding layers, two 7×7 convolutional layers and a tangent function.
- **Image Discriminator**: It contains two discriminators at different scales, which are similar to [50]. For each discriminator it is composed of five convolutional blocks. The first block has a 4×4 convolutional layer and LeakyReLU. Each of the next three blocks has a 4×4 convolutional layer, a batch normalization layer and LeakyReLU. The last block only has a 4×4 convolutional layer.

IV. EXPERIMENTS

A. Experimental Setup

1) *Datasets*: We built MIXAMO-SUP as support set for data augmentation, to boost the generality of DFC-Net and organized two datasets, MIXAMO-POSE and EDN-10K, to verify the effectiveness of the proposed DFC-Net for human pose transfer.

- **MIXAMO-POSE**: We randomly chose 4 characters, *Andromeda*, *Liam*, *Remy* and *Stefani*, with 30 different pose sequences from Mixamo. To render the 3D animations into 2D images, we loaded each character performing each pose sequence on a white background into Blender [58], placed two cameras in front of and behind the character, and took the images. We centered the characters in the images according to their keypoints and resized them to 256×256 . MIXAMO-POSE were splitted into training and test sets. For each character, the training set contains 1488 images with 15 poses, and the test set contains 1185 images with 15 other poses.
- **EDN-10K**: We processed and tailored the dataset released by [30] to build the EDN-10K dataset. The original dataset consists of five long target videos, each lasting from 8 minutes to 17 minutes and split into the training and test set. We chose the first four subjects since the subject five only performed less complex dance poses. In each video of the original dataset, a different subject performed a series of different motions, and the camera was fixed to keep the background unchanged. We chose four subjects from the original dataset, uniformly sampled 10k frames as the training set and 1k frames as the test set for each subject, Since the original images have a large resolution of 1024×512 and most areas are the fixed background, we cropped all frames to the middle 512×512 square areas and resized them to 256×256 .
- **MIXAMO-SUP**: For data augmentation, we built a *support set* by rendering 15684 images of six new characters from Mixamo [29] with another 15 unseen poses in the same way as MIXAMO-POSE. Since it is unnecessary to

Method	<i>Andromeda</i>	<i>Liam</i>	<i>Remy</i>	<i>Stefani</i>	Average
NN	24.9047	28.4846	27.1801	24.8609	26.3576
CycleGAN	27.5520	29.9436	28.2237	22.7682	27.1219
Pix2Pix	23.9370	23.5610	24.0687	21.5841	23.2877
EDN	24.3244	23.1203	23.9229	35.0930	26.6151
LWG	24.2905	22.8587	22.9707	22.0910	23.0527
MKN	30.5934	39.3444	29.4817	24.1297	30.8873
FOMM	27.7809	29.0469	27.4474	25.3934	28.6544
Ours	23.8539	21.7328	22.0763	21.2587	22.2304

TABLE I: Comparisons on MIXAMO-POSE in terms of MSE with the best results (lowest values) in bold.

Method	<i>Andromeda</i>	<i>Liam</i>	<i>Remy</i>	<i>Stefani</i>	Average
NN	0.7357	0.7265	0.7487	0.7411	0.7380
CycleGAN	0.7205	0.7154	0.7377	0.7753	0.7372
Pix2Pix	0.7784	0.7955	0.7932	0.8069	0.7935
EDN	0.7817	0.7931	0.7926	0.8058	0.7933
LWG	0.7613	0.7912	0.7887	0.7858	0.7817
MKN	0.7076	0.6874	0.7531	0.7753	0.7308
FOMM	0.7165	0.7404	0.7538	0.7464	0.7392
Ours	0.7726	0.8040	0.8057	0.8071	0.7973

TABLE II: Comparisons on MIXAMO-POSE in terms of SSIM with best results (highest values) in bold.

Method	<i>Andromeda</i>	<i>Liam</i>	<i>Remy</i>	<i>Stefani</i>	Average
NN	34.4420	34.0575	34.3865	34.3977	34.3209
CycleGAN	33.7903	33.4230	33.6786	34.6130	33.8762
Pix2Pix	34.4049	34.5167	34.3875	34.8497	34.5397
EDN	34.3524	34.5882	34.4214	34.7247	34.5217
LWG	34.3426	34.6762	34.6183	34.7519	34.5972
MKN	33.6626	32.8841	33.7487	34.4779	33.6933
FOMM	33.7777	33.5912	33.8337	34.1919	33.8486
Ours	34.4336	34.8798	34.7823	34.9303	34.7565

TABLE III: Comparisons on MIXAMO-POSE in terms of PSNR with the best results (highest values) in bold.

Method	MSE(↓)	PSNR(↑)	SSIM(↑)
NN	26.3576	34.3209	0.7380
CycleGAN	27.1219	33.8762	0.7372
Pix2Pix	23.2877	34.5397	0.7935
EDN	26.6151	34.5217	0.7933
LWG	23.0527	34.5972	0.7817
MKN	30.8873	33.6933	0.7308
FOMM	28.6544	33.8486	0.7392
Ours	22.2304	34.7565	0.7973

TABLE IV: Comparisons of average results on MIXAMO-POSE with best results in bold.

contain the same person as the target person image, DFC-Net leveraged the support set as the source person images x_s . When training on both EDN-10K and MIXAMO-POSE, we use MIXAMO-SUP as the support set. Note that MIXAMO-SUP has a totally different distribution from EDN-10K but still gains a huge improvement shown in Section IV-C.

Note that the experiments on EDN-10K only include the pose transfer on the same person because the ground-truth of different people carrying the same pose are unavailable. For

MIXAMO-POSE, since we can manipulate different characters to do the same action, the experiments include the pose transfer both on the different people, e.g., transfer the unseen pose of *Liam* to *Andromeda*, and the same person, e.g., transfer the unseen pose of *Andromeda* to herself.

2) *Baseline Methods*: We compared our DFC-Net with the following competitive baselines:

- **Nearest Neighbors (NN)**: For each source person image x_s , we chose the image x' in the training set \mathcal{D}_{tr} with the lowest mean square error (MSE) between the pose information $P(x_s)$ and $P(x')$ as x_{syn} .

$$x_{syn} = \arg \min_{x' \in \mathcal{D}_{tr}} \|P(x_s) - P(x')\|_2^2. \quad (10)$$

The pose information was extracted by the same Pose Estimator as in our method.

- **Pose-guided Methods**: We chose CycleGAN [12], Pix2Pix [11] and Everybody Dance Now (EDN) [30] as the baselines. They all took the skeleton images as input instead of the original images, we employed a pre-trained pose estimator [38] to extract keypoints, used OpenCV [59] to connect pairs of keypoints with different colors to generate the skeleton images. To ensure fair comparisons, the face GAN and face keypoint estimator in EDN were not adopted in our implementation, as they are independent components and can be seamlessly adopted by other learning-based baselines.
- **Spatial Transformation Methods**: We selected Liquid Warping GAN (LWG) [23], Monkey-Net (MKN) [45] and First Order Motion Model (FOMM) [46]. LWG calculates the flow fields with additional 3D human models and integrates the human pose transfer, appearance transfer and novel view synthesis into one unified framework. MKN and FOMM are both object-agnostic frameworks using learned keypoints to generate image animation in a self-supervised fashion.

3) *Evaluation Metrics*: We evaluated the quality of the synthesized images with three commonly used metrics:

- **MSE**: The mean squared error between the values of pixels of synthesized images and ground-truth images. *Lower* MSE values are better.
- **PSNR**: The peak signal-to-noise ratio, which provides an empirical measure of the quality of synthesized images regarding ground-truth images. *Higher* PSNR values are better.
- **SSIM**: Structural similarity [60], which is another perceptual metric that quantifies the quality of synthesized images given ground-truth images and focuses more on structural information (e.g., light). *Higher* SSIM values are better.

We calculated the average scores among all pairs of synthesized and ground-truth images on the test set. On MIXAMO-POSE, for each character as the target person, we reported the average metrics of 4 different characters as the source person. While on EDN-10K, we reported metrics of the task on the same person for every subject.

Method	<i>Subject1</i>	<i>Subject2</i>	<i>Subject3</i>	<i>Subject4</i>	Average
NN	54.9448	36.2267	55.2041	26.2531	43.1572
CycleGAN	64.1959	77.4336	70.3681	52.5171	66.1287
Pix2Pix	58.3633	43.0771	62.0203	24.1688	46.9074
EDN	56.3549	36.3887	55.9625	21.5724	42.5696
LWG	51.6246	43.2884	53.4031	21.4314	42.4368
MKN	48.1603	30.9902	47.6255	21.6634	37.1098
FOMM	46.2852	30.7603	51.1431	21.2709	37.3648
Ours	45.2043	30.4782	48.5436	20.7248	36.2377

TABLE V: Comparisons on EDN-10k in terms of MSE with the best results (lowest values) in bold.

Method	<i>Subject1</i>	<i>Subject2</i>	<i>Subject3</i>	<i>Subject4</i>	Average
NN	0.6138	0.8253	0.7616	0.8437	0.7611
CycleGAN	0.5256	0.4911	0.5869	0.7821	0.5964
Pix2Pix	0.6238	0.8040	0.7585	0.8767	0.7658
EDN	0.6205	0.8445	0.8233	0.8939	0.7956
LWG	0.6394	0.8375	0.7434	0.8634	0.7709
MKN	0.7007	0.8503	0.8030	0.8904	0.8111
FOMM	0.6645	0.8445	0.7896	0.8649	0.7908
Ours	0.7083	0.8670	0.8241	0.9083	0.8269

TABLE VI: Comparisons on EDN-10k in terms of SSIM with the best results (highest values) in bold.

Method	<i>Subject1</i>	<i>Subject2</i>	<i>Subject3</i>	<i>Subject4</i>	Average
NN	30.7957	32.6439	31.3307	34.2481	32.2546
CycleGAN	30.0577	29.2421	29.7007	31.3398	30.0851
Pix2Pix	30.6020	32.0304	30.5843	34.6860	31.9757
EDN	30.7109	32.8639	30.9957	35.0369	32.4019
LWG	31.0085	31.7812	31.0503	35.0118	32.2129
MKN	31.3094	33.2530	30.6493	34.9108	32.5306
FOMM	31.5272	33.3145	31.3099	34.9612	32.7782
Ours	31.5978	33.3509	31.4159	35.0718	32.8591

TABLE VII: Comparisons on EDN-10k in terms of PSNR with the best results (highest values) in bold.

Method	MSE(\downarrow)	PSNR(\uparrow)	SSIM(\uparrow)
NN	43.1572	32.2546	0.7611
CycleGAN	66.1287	30.0851	0.5964
Pix2Pix	46.9074	31.9757	0.7658
EDN	42.5696	32.4019	0.7956
LWG	42.4368	32.2129	0.7709
MKN	37.1098	32.5306	0.8111
FOMM	37.3648	32.7782	0.7908
Ours	36.2377	32.8591	0.8269

TABLE VIII: Comparisons of average results on EDN-10k with best results in bold.

B. Quantitative Evaluations

1) *Results on MIXAMO-POSE*: Tables I, II and III respectively show the quantitative results of pose transfer in terms of MSE, SSIM and PSNR on the MIXAMO-POSE dataset. Summarizing the aboving tables, Table IV shows the average quantitative results of pose transfer in terms of three metrics on MIXAMO-POSE. We obtained the empirical results clearly demonstrated the effectiveness of DFC-Net on animation images:

	KA	\mathcal{L}_{sc}	\mathcal{L}_{mc}	\mathcal{L}_{sup}	MSE(\downarrow)	PSNR(\uparrow)	SSIM(\uparrow)
1					52.5749	30.9361	0.6595
2	✓				50.7810	31.0860	0.6676
3	✓	✓			49.3831	31.2043	0.6742
4	✓		✓		49.8352	31.1662	0.6710
5	✓	✓	✓		48.6431	31.2714	0.6796
6		✓	✓	✓	46.3699	31.4801	0.6937
7	✓	✓	✓	✓	45.2043	31.5978	0.7083

TABLE IX: Ablation studies on *Subject1* from EDN-10k. KA denotes the Keypoint Amplifier.

	KA	\mathcal{L}_{sc}	\mathcal{L}_{mc}	\mathcal{L}_{sup}	MSE(\downarrow)	PSNR(\uparrow)	SSIM(\uparrow)
1					26.4595	33.9856	0.7605
2	✓				24.7312	34.2838	0.7726
3	✓	✓			23.7580	34.4666	0.7830
4	✓		✓		22.6160	34.6913	0.8011
5	✓	✓	✓		21.9509	34.8292	0.8032
6		✓	✓	✓	22.0240	34.8047	0.8031
7	✓	✓	✓	✓	21.7328	34.8798	0.8040

TABLE X: Ablation studies on *Liam* from MIXAMO-POSE. KA denotes the Keypoint Amplifier.

- Our DFC-Net outperformed all competing baselines regarding all three metrics on average. Notably in terms of MSE, DFC-Net outperformed the second best by 0.82.
- MKN and FOMM dropped their performance when they transferred the pose between different people. It is difficult for them to extract keypoints features without a pre-trained pose estimator when the source person was not in the training dataset.

2) *Results on EDN-10k*: Tables V, VI and VII depict results in terms of MSE, SSIM and PSNR on the EDN-10k dataset. Table VIII depicts the average results of 4 subjects on the EDN-10k dataset. The experimental results validated the advances of DFC-Net for real images:

- Our method consistently outperformed all the baseline methods on all subjects. For instance, our method achieved the highest average SSIM of 0.8269 for all subjects, while no other methods except MKN got SSIM score greater than 0.8.
- We observed that MKN and FOMM also provided good results, especially on MSE metric, e.g., 37.1098 and 37.3648 in Table VIII.

C. Ablation Study

To better understand the merits of designs of DFC-Net, we conducted detailed ablation studies on *Subject1* from EDN-10k and *Liam* from MIXAMO-POSE. The evaluation results are shown in Tables IX and X.

1) *Keypoint Amplifier*: The results in the second row versus those in the first row showed that the keypoint amplifier strengthened the performance of pose transfer. Even with the consistency losses and support set (rows 6 and 7), it continuously reduced the interference of the noise on the keypoint heatmaps.

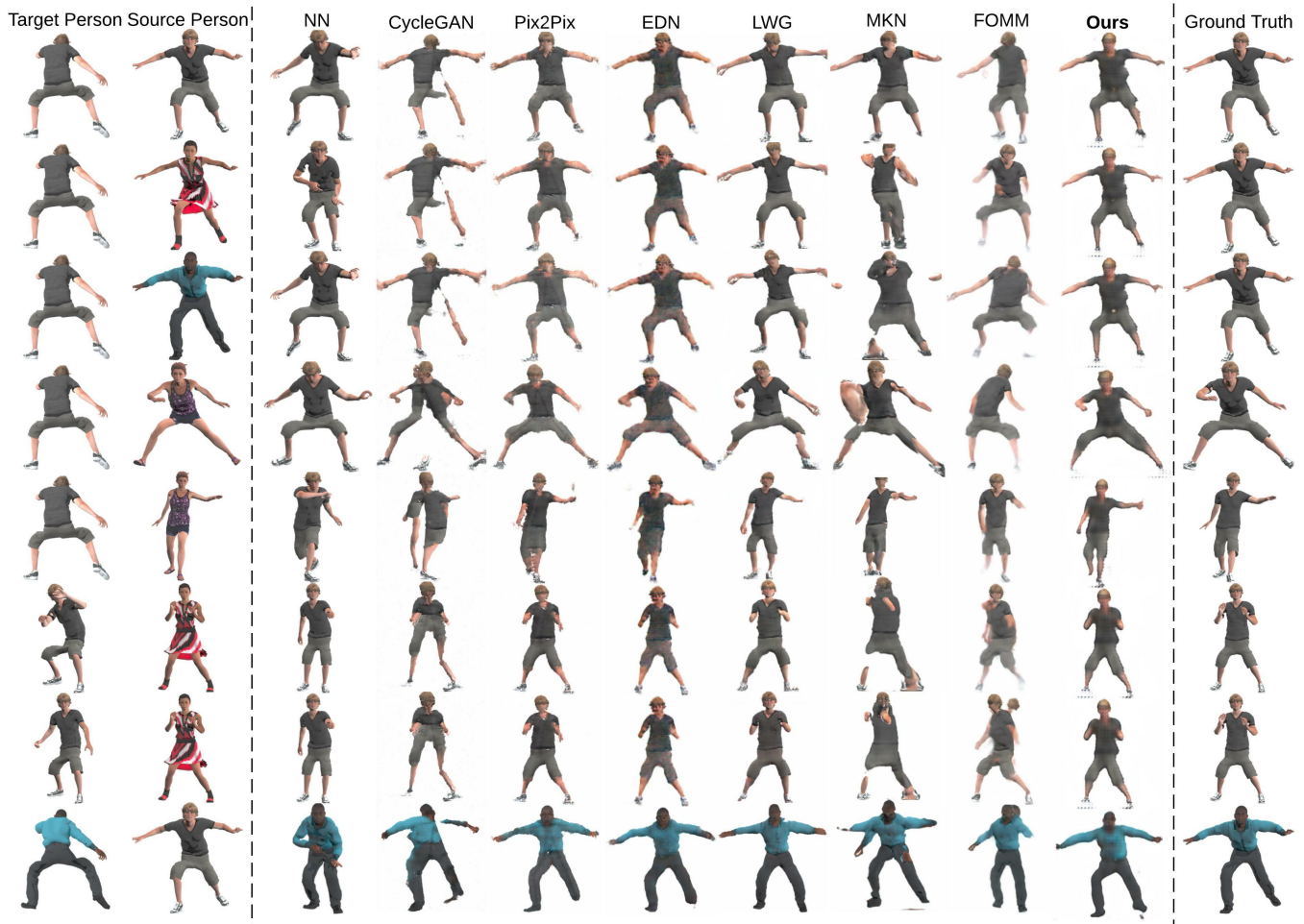


Fig. 2: Visualizations of motion transfer with different characters and various motions on MIXAMO-POSE. The columns from left to right show target persons, source persons, results of different methods, and ground truth, respectively.

2) *Consistency Losses*: We explored the effects of consistency losses on the task of pose transfer. Considering the different results between the second row and the third row, the static feature consistency loss \mathcal{L}_{sc} boosted the pose transfer task and verified its validity. Moreover, the performance variations between the second row and the fourth row clearly evidenced the advantages of pose feature consistency loss \mathcal{L}_{mc} .

3) *Support Set with Augmented Consistency Loss*: Finally, we added the support set and utilized the augmented consistency loss \mathcal{L}_{sup} during the training. The comparisons among the final row and other rows notably indicated that the support set could improve the generalization ability and the robustness of our model, especially when the poses of the source person are closer to the poses in the support set. The support set provided more negative examples besides the original training set and could help the discriminator to form an accurate boundary, which could further strengthen the performance of the generator.

D. Qualitative Results

We further highlighted the superiority of our proposed approach by showing and contrasting the visualizations of synthesized results of all models on MIXAMO-POSE and EDN-

10K, respectively. In addition, we presented the visualizations of the ablation comparisons for *Subject1* on EDN-10K to indicate the effectiveness of components of DFC-Net.

1) *Visual comparisons on MIXAMO-POSE*: As depicted in Figure 2, we employed multiple target persons and source persons with various poses that were different from those in the training set of the MIXAMO-POSE. Compared with the aforementioned baselines, DFC-Net offered better transfer results and alleviated their drawbacks on synthesizing body parts, clothes, faces, just name a few. We illustrate details as follows:

- Firstly, only DFC-Net generated the left hand of *Liam* at the 1st and 2nd rows while there were only the arm in results of other baselines.
- Meanwhile, images produced by EDN had stale colors and lots of noisy pixels in terms of clothes and faces, and it failed to capture the details of shoes at the 3rd row since the color of shoes is white and is easily confused with the background.
- Moreover, even the image results of NN are more clear and not blurry, the NN method always made incorrect pose transfer since it can solely synthesize poses existed in the training set.

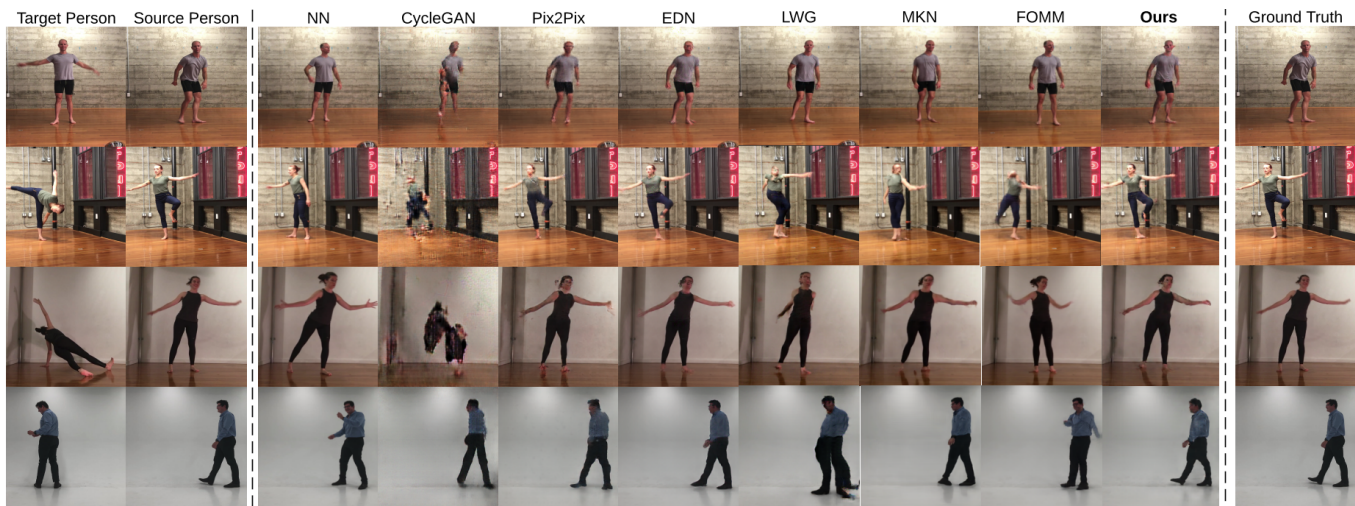


Fig. 3: Visualizations of pose transfer with different characters and various poses on EDN-10K. The columns from left to right show target persons, source persons, results of different methods, and ground truth, respectively.

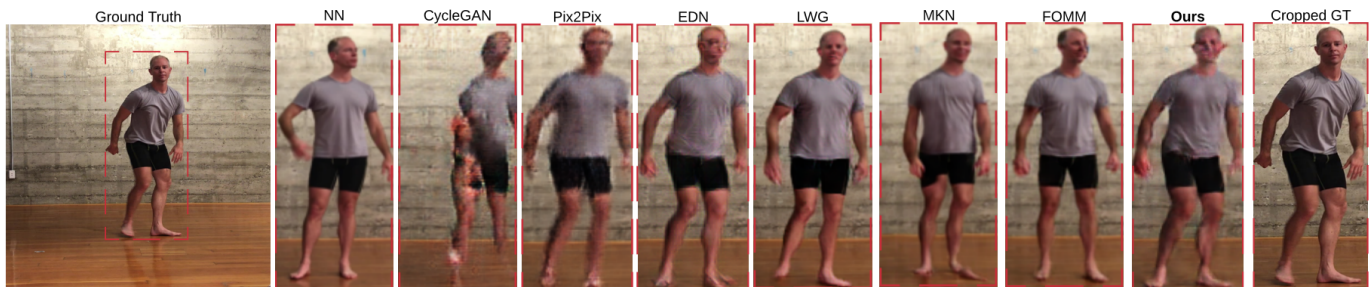


Fig. 4: Visualizations of *Subject1* from EDN-10K with more details. The image in the first left column is the source image and ground truth. We did not show the target image (i.e., the same person with different pose) due to space limitation and cropped the results to the areas surrounded by the red dash lines.

- The CycleGAN could provide similar poses compared with the ground-truths, the poses were distorted and the qualities of corresponding images were constantly degraded.
- Besides, though the Pix2Pix and EDN could synthesize the target persons with the desired poses, some body parts (e.g., arms, hands) generated by Pix2Pix were severely corrupted.

2) *Visual comparisons on EDN-10K*: We also provided visualization results on EDN-10K in Figure 3 and cropped the results in Figure 4 with more details, and DFC-Net synthesized real person image results with better qualities, which clearly indicated the effectiveness of our method as well. For instance:

- The results produced by Pix2Pix and EDN were more blurry and there was an aliasing effect on the edges of the subject in the Pix2Pix result.
- Sometimes NN could generate images that are closer to the ground-truths, e.g. image of *Subject3* at the third row of Figure 3, since the number of images in the training set increases from 1488 to 10000. But people could still easily determine that the poses of the generated images are different from the ground-truths.
- In addition, EDN showed better image results than Pix2Pix did. In the third row of Figure 3, we noticed

that the image of *Subject3*, synthesized by Pix2Pix, had much noise in the subject’s hair. On the contrary, the result of EDN was smoother and more realistic, but they lacked many details compared with DFC-Net, especially the face part was still twisted.

- As depicted in Figure 4, we observed that the synthesized images of our method contained more details, including the clear face, wrinkles on clothes, etc.

3) *Visual ablation studies on Subject1*: We presented the visualization of the ablation study results on *Subject1* in Figure 5. In which we observed that each component has different degrees of improvement to the results, including clear head, hand gesture, etc. Specifically:

- As shown in the column of setting 7, DFC-Net with full components synthesized images with more accurate details and better qualities.
- The results produced by setting 1, which does not have the Keypoint Amplifier, have much noise then other settings, especially near the head area.

V. CONCLUSION

In this paper, we proposed DFC-Net, a novel network with disentangled feature consistencies for human pose transfer. We

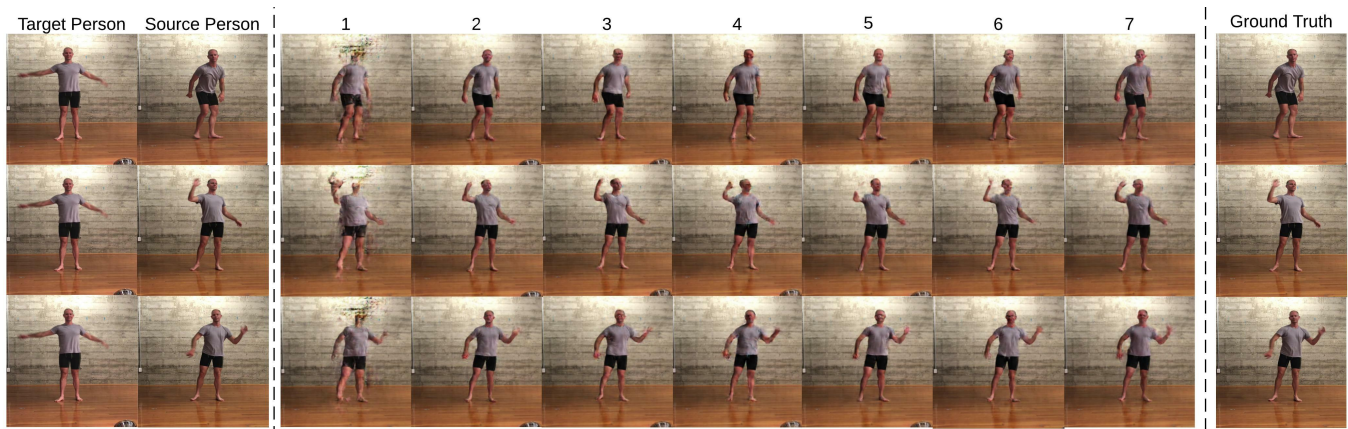


Fig. 5: Visualizations of *Subject1* from EDN-10K. The columns from left to right show target persons, source persons, results of 6 different settings in ablation studies, and ground truth, respectively. The indices of each column are the same as in the Table X.

introduce two disentangled feature consistency losses to enforce the pose and static information to be consistent between the synthesized and real images. Besides, we leverage the keypoint amplifier to denoise the keypoint heatmaps and make it easier to extract the pose features. Moreover, we show that the support set MIXAMO-SUP containing different subjects with unseen poses can boost the pose transfer performance and enhance the robustness of the model. To enable the accurate evaluation of pose transfer between different people, we collect an animation character dataset MIXAMO-POSE. Results on both animation and real image datasets, MIXAMO-POSE and EDN-10K, consistently demonstrated the effectiveness of the proposed model.

REFERENCES

- [1] H.-Y. Tung, H.-W. Tung, E. Yumer, and K. Fragkiadaki, "Self-supervised learning of motion capture," in *NIPS*, 2017.
- [2] L. Liu, W. Xu, M. Zollhoefer, H. Kim, F. Bernard, M. Habermann, W. Wang, and C. Theobalt, "Neural rendering and reenactment of human actor videos," *ACM Transactions on Graphics*, 2019.
- [3] L. Wei, S. Zhang, H. Yao, W. Gao, and Q. Tian, "Glad: Global-local alignment descriptor for scalable person re-identification," *IEEE Transactions on Multimedia*, 2019.
- [4] S. Xia, L. Gao, Y.-K. Lai, M.-Z. Yuan, and J. Chai, "A survey on human performance capture and animation," *Journal of Computer Science and Technology*, 2017.
- [5] T. B. Moeslund, A. Hilton, and V. Krüger, "A survey of advances in vision-based human motion capture and analysis," *Computer vision and image understanding*, 2006.
- [6] H. Zhan, C. Yi, B. Shi, J. Lin, L.-Y. Duan, and A. C. Kot, "Pose-normalized and appearance-preserved street-to-shop clothing image generation and feature learning," *IEEE Transactions on Multimedia*, 2021.
- [7] I. Goodfellow, J. Pouget-Abadie, M. Mirza, B. Xu, D. Warde-Farley, S. Ozair, A. Courville, and Y. Bengio, "Generative adversarial nets," in *NIPS*, 2014.
- [8] H. Mo, L. Liu, W. Zhu, S. Yin, and S. Wei, "Face alignment with expression- and pose-based adaptive initialization," *IEEE Transactions on Multimedia*, 2019.
- [9] Y. Liu, W. Chen, L. Liu, and M. S. Lew, "Swappan: A multistage generative approach for person-to-person fashion style transfer," *IEEE Transactions on Multimedia*, 2019.
- [10] X. Gu, J. Yu, Y. Wong, and M. S. Kankanhalli, "Toward multi-modal conditioned fashion image translation," *IEEE Transactions on Multimedia*, 2021.
- [11] P. Isola, J.-Y. Zhu, T. Zhou, and A. A. Efros, "Image-to-image translation with conditional adversarial networks," in *CVPR*, 2017.
- [12] J.-Y. Zhu, T. Park, P. Isola, and A. A. Efros, "Unpaired image-to-image translation using cycle-consistent adversarial networks," in *ICCV*, 2017.
- [13] L. Ma, X. Jia, Q. Sun, B. Schiele, T. Tuytelaars, and L. Van Gool, "Pose guided person image generation," in *NIPS*, 2017.
- [14] L. Ma, Q. Sun, S. Georgoulis, L. Van Gool, B. Schiele, and M. Fritz, "Disentangled person image generation," in *CVPR*, 2018.
- [15] Y. Li, C. Huang, and C. C. Loy, "Dense intrinsic appearance flow for human pose transfer," in *CVPR*, 2019.
- [16] P. Esser, E. Sutter, and B. Ommer, "A variational u-net for conditional appearance and shape generation," in *CVPR*, 2018.
- [17] A. Siarohin, E. Sangineto, S. Lathuilière, and N. Sebe, "Deformable gans for pose-based human image generation," in *CVPR*, 2018.
- [18] N. Neverova, R. Alp Guler, and I. Kokkinos, "Dense pose transfer," in *ECCV*, 2018.
- [19] A. Grigorev, A. Sevastopolsky, A. Vakhitov, and V. Lempitsky, "Coordinate-based texture inpainting for pose-guided human image generation," in *CVPR*, 2019.
- [20] Z. Zhu, T. Huang, B. Shi, M. Yu, B. Wang, and X. Bai, "Progressive pose attention transfer for person image generation," in *CVPR*, 2019.
- [21] Y. Ren, X. Yu, J. Chen, T. H. Li, and G. Li, "Deep image spatial transformation for person image generation," in *CVPR*, 2020.
- [22] T.-C. Wang, M.-Y. Liu, J.-Y. Zhu, G. Liu, A. Tao, J. Kautz, and B. Catanzaro, "Video-to-video synthesis," in *NIPS*, 2018.
- [23] W. Liu, Z. Piao, J. Min, W. Luo, L. Ma, and S. Gao, "Liquid warping gan: A unified framework for human motion imitation, appearance transfer and novel view synthesis," in *ICCV*, 2019.
- [24] Z. Cao, G. Hidalgo Martinez, T. Simon, S. Wei, and Y. A. Sheikh, "Openpose: Realtime multi-person 2d pose estimation using part affinity fields," *IEEE Transactions on Pattern Analysis and Machine Intelligence*, 2019.
- [25] T.-Y. Lin, M. Maire, S. Belongie, J. Hays, P. Perona, D. Ramanan, P. Dollár, and C. L. Zitnick, "Microsoft coco: Common objects in context," in *ECCV*, 2014.
- [26] L. Zheng, L. Shen, L. Tian, S. Wang, J. Wang, and Q. Tian, "Scalable person re-identification: A benchmark," in *ICCV*, 2015.
- [27] Z. Liu, P. Luo, S. Qiu, X. Wang, and X. Tang, "Deepfashion: Powering robust clothes recognition and retrieval with rich annotations," in *CVPR*, 2016.
- [28] K. Aberman, R. Wu, D. Lischinski, B. Chen, and D. Cohen-Or, "Learning character-agnostic motion for motion retargeting in 2d," *ACM Transactions on Graphics (TOG)*, 2019.
- [29] Adobe Systems Inc., <https://www.mixamo.com>, 2018, accessed: 2018-12-27.
- [30] C. Chan, S. Ginosar, T. Zhou, and A. A. Efros, "Everybody dance now," in *ICCV*, 2019.
- [31] M. Mirza and S. Osindero, "Conditional generative adversarial nets," *arXiv preprint arXiv:1411.1784*, 2014.
- [32] G. E. Hinton and R. R. Salakhutdinov, "Reducing the dimensionality of data with neural networks," *science*, 2006.
- [33] Z. Yi, H. Zhang, P. Tan, and M. Gong, "Dualgan: Unsupervised dual learning for image-to-image translation," in *ICCV*, 2017.

- [34] Y. Hoshen and L. Wolf, "Identifying analogies across domains," in *ICLR*, 2018.
- [35] M.-Y. Liu, T. Breuel, and J. Kautz, "Unsupervised image-to-image translation networks," in *NIPS*, 2017.
- [36] K. Bousmalis, N. Silberman, D. Dohan, D. Erhan, and D. Krishnan, "Unsupervised pixel-level domain adaptation with generative adversarial networks," in *CVPR*, 2017.
- [37] X. Huang, M.-Y. Liu, S. Belongie, and J. Kautz, "Multimodal unsupervised image-to-image translation," in *ECCV*, 2018.
- [38] Z. Cao, T. Simon, S.-E. Wei, and Y. Sheikh, "Realtime multi-person 2d pose estimation using part affinity fields," in *CVPR*, 2017.
- [39] H. Dong, X. Liang, K. Gong, H. Lai, J. Zhu, and J. Yin, "Soft-gated warping-gan for pose-guided person image synthesis," in *NIPS*, 2018.
- [40] M. Jaderberg, K. Simonyan, A. Zisserman *et al.*, "Spatial transformer networks," in *NIPS*, 2015.
- [41] H. Zhang and X. He, "Deep free-form deformation network for object-mask registration," in *ICCV*, 2017.
- [42] C.-H. Lin and S. Lucey, "Inverse compositional spatial transformer networks," in *CVPR*, 2017.
- [43] W. Jiang, W. Sun, A. Tagliasacchi, E. Trulls, and K. M. Yi, "Linearized multi-sampling for differentiable image transformation," in *ICCV*, 2019.
- [44] G. Balakrishnan, A. Zhao, A. V. Dalca, F. Durand, and J. Guttag, "Synthesizing images of humans in unseen poses," in *CVPR*, 2018.
- [45] A. Siarohin, S. Lathuilière, S. Tulyakov, E. Ricci, and N. Sebe, "Animating arbitrary objects via deep motion transfer," in *CVPR*, 2019.
- [46] A. Siarohin, S. Lathuilière, S. Tulyakov, E. Ricci, and N. Sebe, "First order motion model for image animation," in *NIPS*, 2019.
- [47] M. Loper, N. Mahmood, J. Romero, G. Pons-Moll, and M. J. Black, "Smpl: A skinned multi-person linear model," *ACM transactions on graphics (TOG)*, 2015.
- [48] C. Si, W. Wang, L. Wang, and T. Tan, "Multistage adversarial losses for pose-based human image synthesis," in *CVPR*, 2018.
- [49] R. Alp Güler, N. Neverova, and I. Kokkinos, "Densepose: Dense human pose estimation in the wild," in *CVPR*, 2018.
- [50] T.-C. Wang, M.-Y. Liu, J.-Y. Zhu, A. Tao, J. Kautz, and B. Catanzaro, "High-resolution image synthesis and semantic manipulation with conditional gans," in *CVPR*, 2018.
- [51] B. Chen, Y. Zhang, H. Tan, B. Yin, and X. Liu, "Pman: Progressive multi-attention network for human pose transfer," *IEEE Transactions on Circuits and Systems for Video Technology*, 2021.
- [52] H. Zheng, L. Chen, C. Xu, and J. Luo, "Unsupervised pose flow learning for pose guided synthesis," *arXiv preprint arXiv:1909.13819*, 2019.
- [53] H. Tang, D. Xu, G. Liu, W. Wang, N. Sebe, and Y. Yan, "Cycle in cycle generative adversarial networks for keypoint-guided image generation," in *Proceedings of the 27th ACM International Conference on Multimedia*, 2019.
- [54] J. Johnson, A. Alahi, and L. Fei-Fei, "Perceptual losses for real-time style transfer and super-resolution," in *ECCV*, 2016.
- [55] K. Simonyan and A. Zisserman, "Very deep convolutional networks for large-scale image recognition," *arXiv preprint arXiv:1409.1556*, 2014.
- [56] —, "Very deep convolutional networks for large-scale image recognition," *arXiv preprint arXiv:1409.1556*, 2014.
- [57] K. He, X. Zhang, S. Ren, and J. Sun, "Deep residual learning for image recognition," in *CVPR*, 2016.
- [58] Blender Online Community, *Blender - a 3D modelling and rendering package*, Blender Foundation, Stichting Blender Foundation, Amsterdam, 2018. [Online]. Available: <http://www.blender.org>
- [59] G. Bradski, "The OpenCV Library," *Dr. Dobb's Journal of Software Tools*, 2000.
- [60] Z. Wang, A. C. Bovik, H. R. Sheikh, E. P. Simoncelli *et al.*, "Image quality assessment: from error visibility to structural similarity," *IEEE transactions on image processing*, 2004.



Kun Wu received his B.S. degree from Beijing Institute of Technology in 2017. He is currently working towards his Ph.D degree in the Department of Electrical Engineering and Computer Science at Syracuse University. His research interests include Machine Learning and Computer Vision.



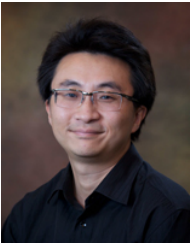
Chengxiang Yin received his B.S. degree from Beijing Institute of Technology in 2016. He is currently working toward his Ph.D degree in the Department of Electrical Engineering and Computer Science at Syracuse University. His research interests include Machine Learning and Computer Vision.



Zhengping Che received the Ph.D. degree in Computer Science from the University of Southern California, Los Angeles, CA, USA, in 2018, and the B.Eng. degree in Computer Science from Tsinghua University, Beijing, China, in 2013. He is now with AI Innovation Center, Midea Group. His current research interests lie in the areas of machine learning, deep learning, computer vision, and time series analysis with broad applications to robot learning.



Bo Jiang received the master degree from the Department of Computer Science, University of Southern California, USA, in 2017. He is a research scientist at Didi Chuxing. His research interests include machine learning and deep learning.



Jian Tang received his Ph.D degree in Computer Science from Arizona State University in 2006. He is an IEEE Fellow and an ACM Distinguished Member. He is with Midea Group. His research interests lie in the areas of AI, IoT, Wireless Networking, Mobile Computing and Big Data Systems. Dr. Tang has published over 160 papers in premier journals and conferences. He received an NSF CAREER award in 2009. He also received several best paper awards, including the 2019 William R. Bennett Prize and the 2019 TCBD (Technical Committee on

Big Data) Best Journal Paper Award from IEEE Communications Society (ComSoc), the 2016 Best Vehicular Electronics Paper Award from IEEE Vehicular Technology Society (VTS), and Best Paper Awards from the 2014 IEEE International Conference on Communications (ICC) and the 2015 IEEE Global Communications Conference (Globecom) respectively. He has served as an editor for several IEEE journals, including IEEE Transactions on Big Data, IEEE Transactions on Mobile Computing, etc. In addition, he served as a TPC co-chair for a few international conferences, including the IEEE/ACM IWQoS'2019, MobiQuitous'2018, IEEE iThings'2015, etc.; as the TPC vice chair for the INFOCOM'2019; and as an area TPC chair for INFOCOM 2017-2018. He is also an IEEE VTS Distinguished Lecturer, and the Chair of the Communications Switching and Routing Committee of IEEE ComSoc.



Zheng Guan is an assistant teacher of Beijing Institute of Technology, graduated from Beijing Institute of Technology Computer Science School. His interest areas are simulation systems, embedded systems, and artificial intelligence.



Gangyi Ding is a professor of Beijing Institute of Technology. His interest areas are simulation systems, embedded systems, and artificial intelligence.